Supporting Information

Nano-assemblies from J-aggregated dyes to improve the selectivity of H_2S-activatable photosensitizer

Dongsheng Zhang, Ming-Chen Xiong, Li-Ya Niu* and Qing-Zheng Yang*

Key Laboratory of Radiopharmaceuticals, Ministry of Education, College of Chemistry, Beijing Normal University, Beijing 100875, P. R. China.

Table of Contents

1 General information

Materials and Instruments

Unless otherwise noted, reagents were used as received from commercial sources. All reagents and solvents used in this study were purchased from the following chemical suppliers: TCI shanghai, ABCR, Acros Organics, Alfa Aesar, Ark Pharm, Combi-Blocks, Oakwood, and Sigma-Aldrich were used as purchased. NMR spectra were obtained on a JEOL spectrometer operating at 400 MHz/600 MHz for ^{1}H and 100 MHz/150 MHz for ^{13}C spectra. Absorption spectra were obtained using UV-3900 HITACHI UV-vis-NIR spectrometer. Fluorescence spectra were determined on Hitachi 4500 spectrophotometer. SEM images of the nanoparticles were obtained using a Hitachi SU-8010 scanning electron microscope. The photoluminescence quantum yield was determined on HAMAMATSU C11347. Dynamic light scattering (DLS) investigations were carried out with a Dyna Pro Nano Star dynamic light scattering detector. High-resolution mass spectra (HRMS) were acquired using an Agilent Technologies 6224 Accurate-Mass time-of-flight spectrometer with either atmospheric pressure chemical ionization (APCI) or electrospray ionization (ESI) ionization sources. Single crystal X-ray diffraction data were collected at 100 K with a SuperNova Rigaku Oxford Diffraction diffractometers with Cu-Kα radiation. X-ray phase analysis of nano-assemblies was performed on an XRD 7000 SHIMADZU diffractometer with automatic program control. Confocal fluorescence imaging was performed on Nikon A1R microscopy. Cell viability test was obtained on a Thermo Scientific Multiskan. Irradiation was performed by using a pure white LED light (6000~6500 K, PLS-LED 100, Perfect Light, Beijing, China).

Preparation of the J-aggregates of BDP-Nit

The J-aggregates of **BDP-Nit** were prepared using a nanoprecipitation method. Briefly, 1 mg **BDP-Nit** and 4 mg F127 were dissolved in THF and fully mixed. Thereafter, the obtained mixed solution was added dropwise into PBS (5 mL) under ultrasonication over 15 min. Residual THF was removed under reduced vacuum.

Crystal Growth

Single crystal of **BDP-Nit** with suitable size for X-Ray analysis was obtained by slow solvent evaporation from the dye solution in CH_2Cl_2/n-heptane mixture for about 2 weeks.

Overall reactive oxygen species (ROS) measurements

2`,7`-dichlorodihydrofluorescein (DCFH) as a nonspecific probe to assess the intracellular overall ROS generation ability of J-aggregates. The DCFH could be oxidized into highly fluorescent DCF by ROS. Typically, the photosensitizers (PS, 3.5 μM) and DCFH (10 μM) were dissolved in the PBS solution. After that, the mixture was exposed to irradiation (pure white LED light source, 30 mW/cm^2). Measurements were carried out by recording the time-depend photoluminescence intensity changes of DCF at ~525 nm in a photoluminescence spectrofluorometer (488 nm excitation).

Cell viability assay

HeLa cells were cultured in DMEM (Dulbecco's Modified Eagle Medium) high glucose medium (Gibco, USA) with humidified atmosphere of 5% CO_2-95% air at 37 °C. All experiments were performed on cells in logarithmic growth phase.

Cellular ROS Generation Assay

Intracellular ROS production of activated J-aggregates was confirmed by DCFH-DA, in which bright green fluorescence was assigned to the generation of total ROS. Typically, HeLa cells with a density of 4×10^5 containing complete DMEM (with FBS) media were incubated in glass culture dish (30 mm) for 24 h. Cells were incubated with J-aggregates for 2 h to allow the cellar uptake, and then incubated with NaHS (0.1 mM) for 5 h to increase H_2S levels to active the J-aggregates. Thereafter, the medium was removed, washed with PBS (pH 7.4) three times, DCFH-DA (working concentration: 10 μM) was added and the cell was for another 30 min. After washed with PBS buffer for three times, the cells medium was replaced with the fresh DMEM (without FBS) and irradiated by LED light (pure white, 50 mW/cm^2). At last, the cell images from DCF were then analyzed were observed via a Laser Scanning Confocal Microscopy to evaluate the ROS generation.

Cytotoxicity Assay

Cytotoxicity of nano-J-aggregate was evaluated by a standard Cell Counting Kit-8 (CCK-8) assay. Typically, HeLa cells were seeded into 96 well plates and incubated with complete DMEM medium for 24 h at 37 °C. For PDT-induced cytotoxicity, cells were incubated with J-aggregates at different concentrations for 2 h. Then, NaHS (0.1 mM) was added and incubate for another 5 h to increase H_2S levels to active the J-aggregates. Thereafter, the medium was removed, and washed with cold PBS buffer for three times. After washing away the excess assemblies, the medium was replaced with 100 μL of complete DMEM medium. For the PDT-treated groups, the cells were irradiated for

10 min. For the control groups, the cells were subjected to darkness all the time. The cells were cultured for an additional 12 h at 37 °C. Then, the cells medium was replaced with the fresh DMEM containing CCK-8 (10%). After treatment for 30 min, the absorbance of the samples was measured at the microplate reader.

Live/Dead staining analysis

HeLa cells with a density of 4×10^5 containing complete DMEM (with FBS) media were incubated in glass culture dish (30 mm) for 24 h. Then, cells were incubated with normal nano-assemblies or activated nano-assemblies (upon incubation with NaSH for 5 h).. After incubation for 2 h, the cells were washed twice with PBS, and subjected to red LED light irradiation for 0, 2, 5 ,10 min. After photoirradiation, cells were incubated for 4 h, and stained with Calcein AM (1.0 μM) and Propidium Iodide (PI; 6.0 μM). After staining for 20 min, the cells were washed with PBS and imaged immediately by CLSM.

2. Synthesis of BPD-Nit and BDP-SH

Synthetic route of **BDP-Nit** was shown in Scheme S1. Iodide BODIPY was prepared as starting material according to the literature[1]. First, thiols-responsive phenol ether function was afforded through the aromatic nucleophilic substitution (S_NAr) between iodide BODIPY fluorescent dye and p-nitrophenol. Then, pyridine was incorporated into the BODIPY by Sonogashira coupling reaction to afford **BDP-Nit**. The detailed synthesis procedures and characterizations are depicted.

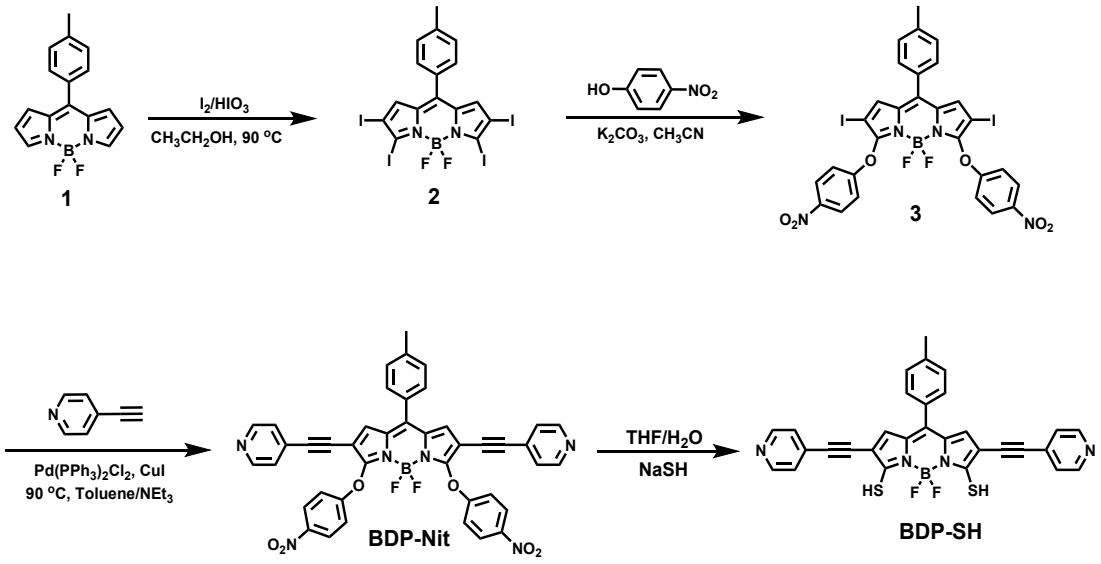

Scheme S1. Synthesis of the target compound **BDP-Nit** and **BDP-SH**.

Synthesis of Compound 3. 785 mg of Iodide BODIPY (1 mmol), 700 mg of p-nitrophenol (5 mmol) and 1.38 g of K_2CO_3 (10 mmol) were mixed in 30 mL CH_3CN. The mixture was stirred and heated at 105 °C for 2 hours. After cooled down, the precipitate was filtered off, washed with water, and dried. The crude product was purified through column chromatography over dichloromethane/n-hexane (2/1, v/v). Yield: 700 mg (88%).

Synthesis of BDP-Nit. Compound 3 (808 mg, 1 mmol), 4-ethynylpyridine (500 mg, 5eq), $Pd(PPh_3)_2Cl_2$ (60 mg) and CuI (6 mg) were added to a mixture of toluene (20 mL) and triethylamine (5 mL) under N_2 atmosphere. The resulting mixture was stirred at 80 °C for about 10 h. After cooling down to room temperature, the solvent was evaporated. The residue as purified by a column chromatography (hexane: dichloromethane: methanol = 10:10:1) to afford brownish red crystals (678.9 mg, yield: 89.5%).

^{1}H NMR (600 MHz, Chloroform-*d*) δ 8.48 – 8.45 (m, 4H), 8.31 – 8.27 (m, 4H), 7.51 (d, J = 8.1 Hz, 2H), 7.41 (d, J = 7.8 Hz, 2H), 7.40 – 7.35 (m, 4H), 7.16 (s, 2H), 6.82 – 6.77 (m, 4H), 2.51 (s, 3H).

^{13}C NMR (150 MHz, Chloroform-*d*) δ 160.70, 159.46, 149.88, 145.31, 144.91, 142.42, 133.86, 130.64, 130.07, 129.81, 129.06, 128.28, 125.84, 124.63, 119.19, 102.66, 94.23, 83.44, 21.61.

Synthesis of BDP-SH

BDP-Nit (758 mg, 1 mmol), NaSH (560 mg, 10 mmol) were added to a mixture of THF (20 mL) and water (5 mL) under N_2 atmosphere. The resulting mixture was stirred at room temperature for about 10 h. Thereafter, 50 mL of DCM was added and then washed with saturated sodium chloride

solution (3 times, 50 mL each). The combined organic layer was dried over sodium sulfate and evaporated under reduced pressure. The residue as purified by a column chromatography (dichloromethane: methanol =10:1) to afford brownish red crystals (400 mg, yield: 80.5%).

^{1}H NMR (400 MHz, Chloroform-*d*) δ 8.64 (d, *J* = 4.9 Hz, 4H), 7.52 (d, *J* = 7.7 Hz, 2H), 7.49 – 7.44 (m, 4H), 7.38 (d, *J* = 7.6 Hz, 2H), 7.30 (d, *J* = 1.6 Hz, 2H), 6.92 (s, 2H), 2.51 (s, 3H).

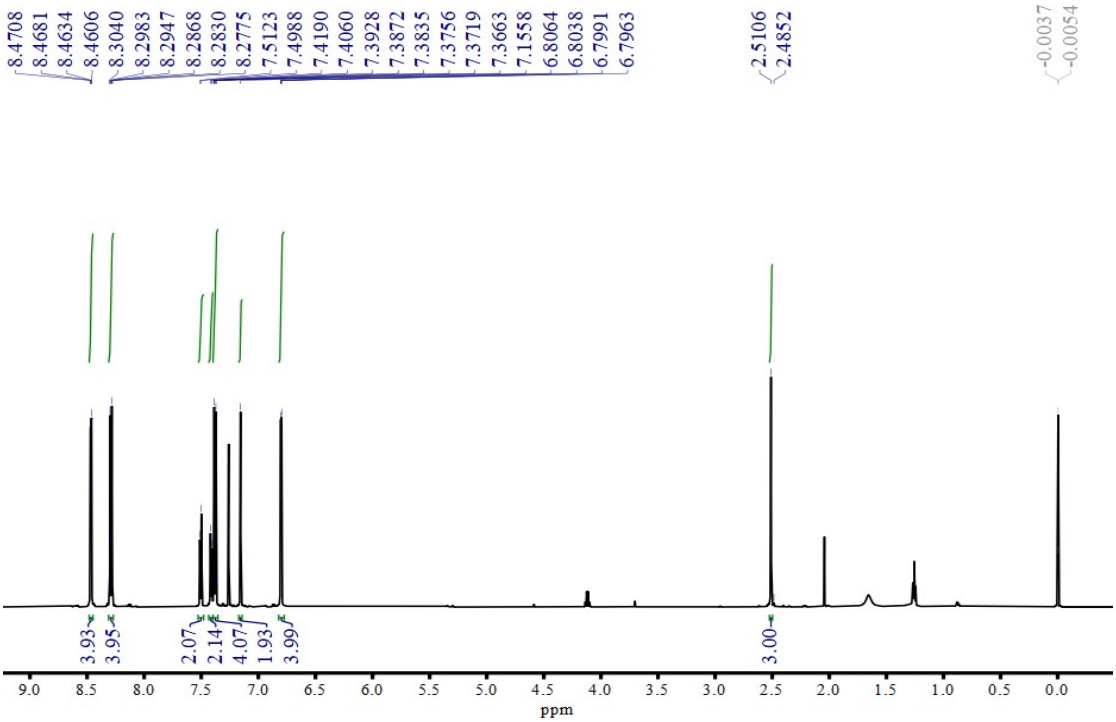

Figure S1. ^{1}H NMR of **BDP-Nit** (Chloroform-*d*).

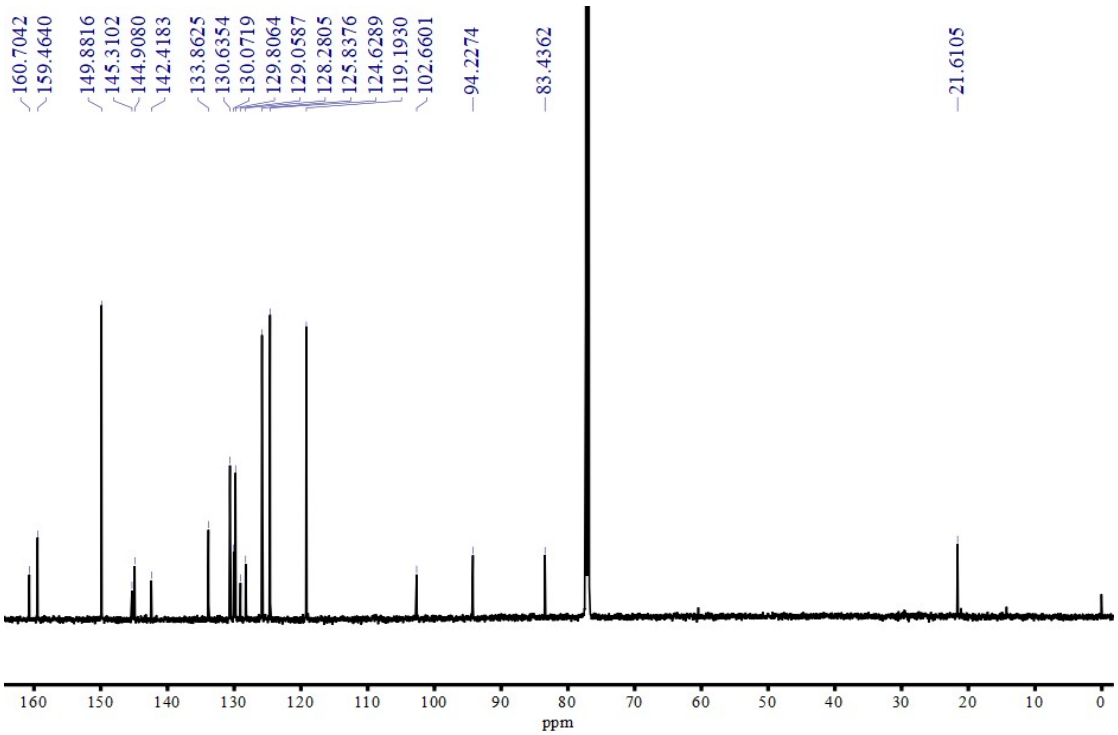

Figure S2. ^{13}C NMR of **BDP-Nit** (Chloroform-*d*).

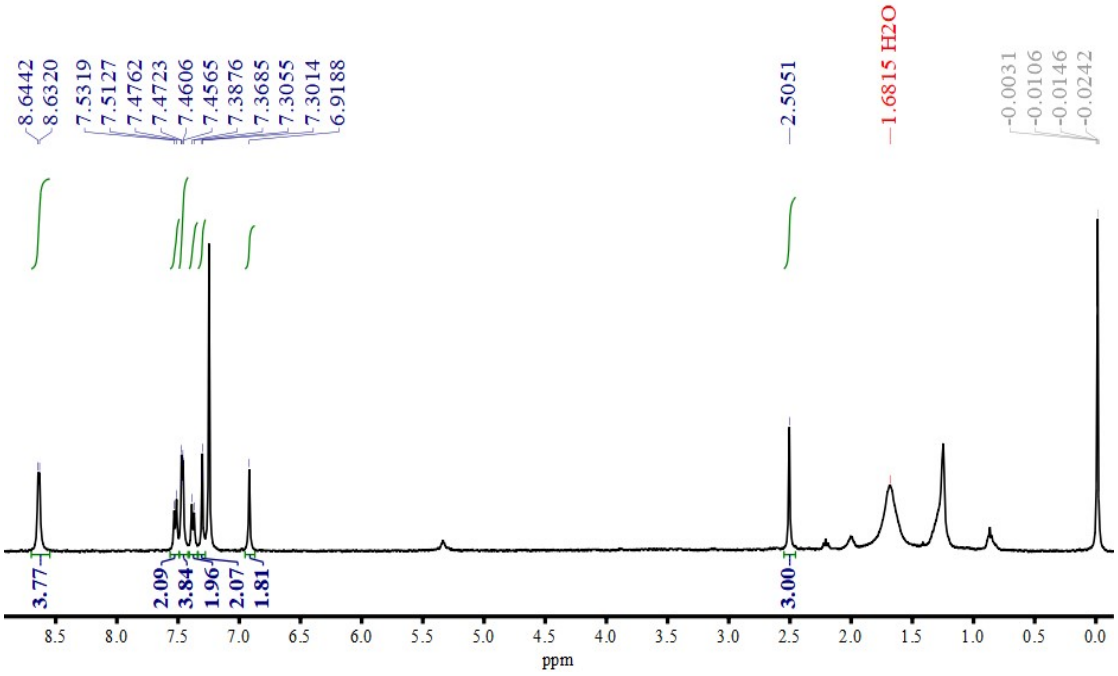

Figure S3. ^{1}H NMR of **BDP-SH** (Chloroform-*d*).

3. Characterization of BDP-Nit nano-assemblies

Table S1. Properties of **BDP-Nit** and **BDP-SH** (activated product of **BDP-Nit**).

Sample	λ_{abs} [a]	ε [b]	λ_{em} [c]	Φ_{PL} [d]
Free **BDP-Nit**[e]	573	6.57	600	26.8
Free **BDP-SH**[f]	623	3.21	635	4.7
Assembled **BDP-Nit**[g]	620	8.64	625	0.4

[a] Maximum absorption wavelength, nm. [b] Molar absorption coefficient, $\times 10^4$ $M^{-1}cm^{-1}$. [c] Maximum fluorescence emission wavelength, in nm. [d] Photoluminescence quantum yield (%). [e] DCM. [f] DCM. [g] H_2O.

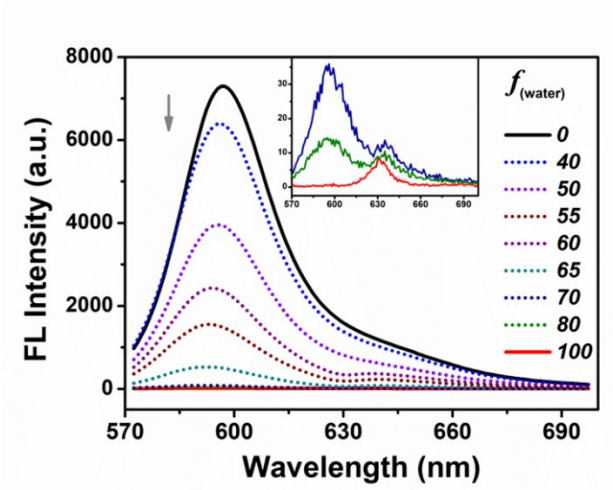

Figure S4. Fluorescence spectra of **BDP-Nit** in MeOH/water mixture with different water fractions (*f* water, vol %) from 0 to 100% (Ex, 560 nm).

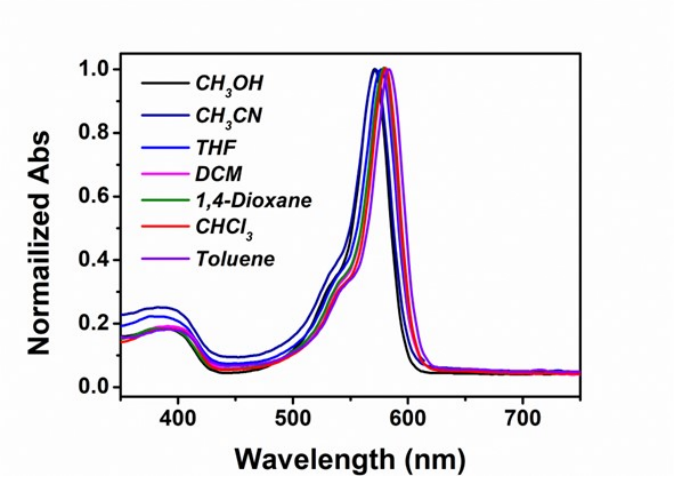

Figure S5. UV-visible absorption spectra of BDP-Nit in different solutions.

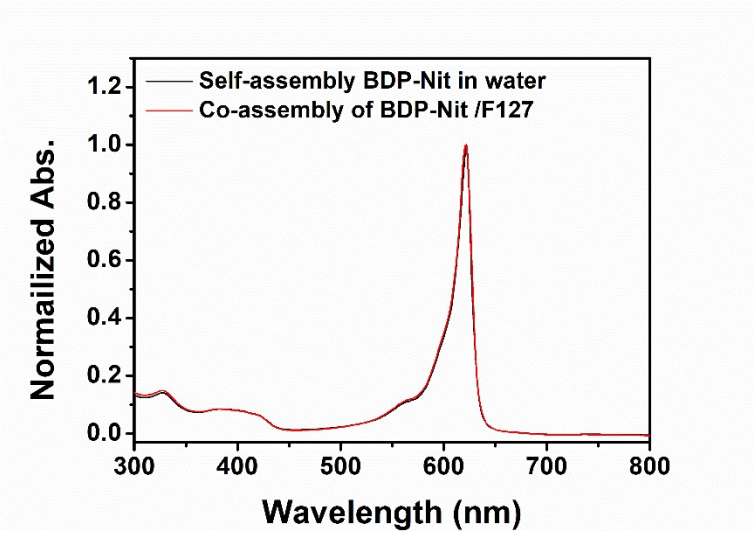

Figure S6. UV-visible absorption spectra of self-assembly of **BDP-Nit** in water and co-assembly of BDP-Nit/F127.

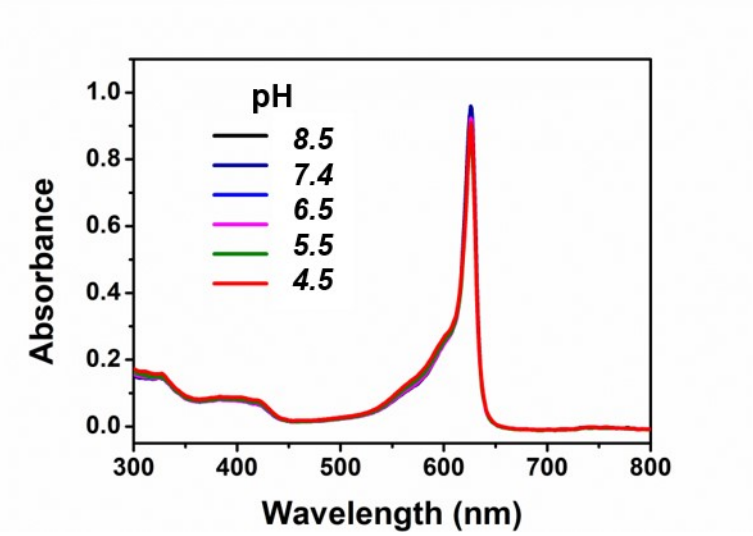

Figure S7. UV-visible absorption spectra of aqueous dispersion of BDP-Nit assemblies with different pH.

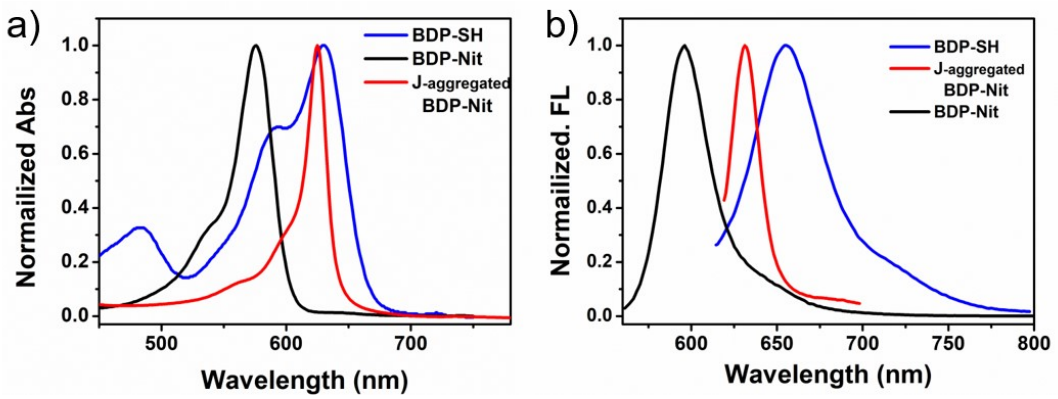

Figure S8. Normalized a) absorption and b) fluorescence of BDP-Nit in DCM, J-aggregated co-assembly of BDP-Nit/F127 dispersed in water and BDP-SH in DCM.

4. Dynamic measurement of the absorption responses towards bio-thiols

(1) Free BDP-Nit: **BDP-Nit** in monomer form shows insufficient selectivity towards H_2S.

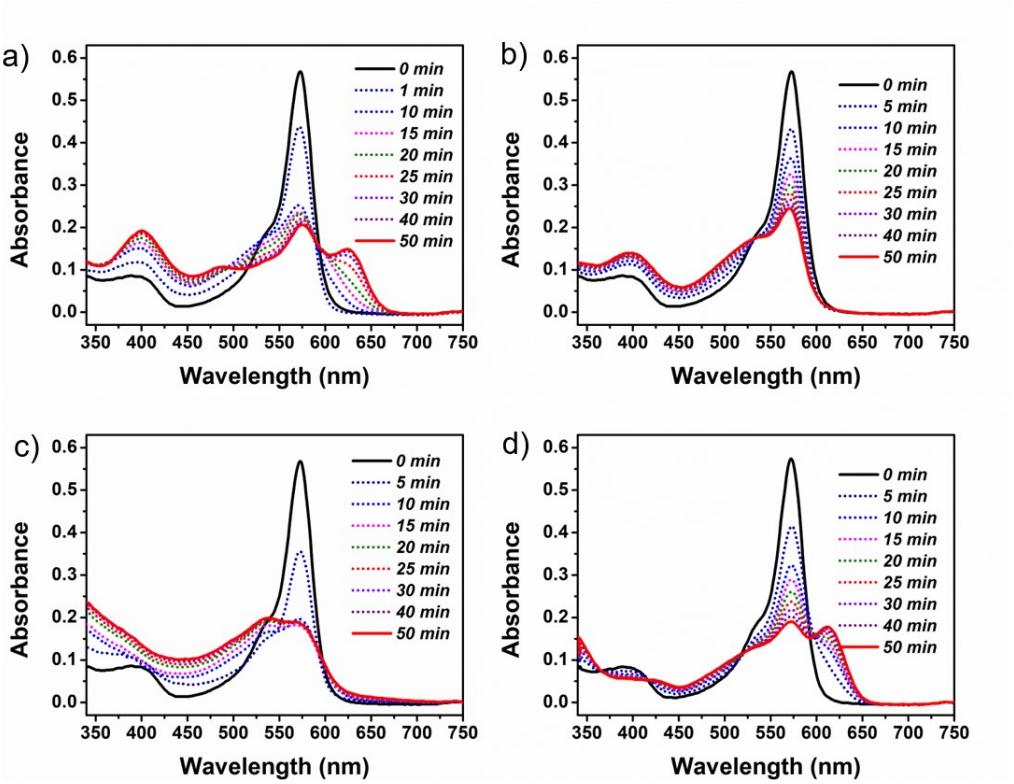

Figure S9. Time-dependent absorption responses of free **BDP-Nit** (9 μM) to (a) NaHS (100 μM), (b) Cys (1 mM), (c) Hcy (1 mM), and (d) GSH (10 mM) in CH_3CN/H_2O (4:1, v/v).

(2) J-aggregated BDP-Nit **(nano-assemblies)*:*** **BDP-Nit** in J-aggregate form shows high selectivity towards H_2S.

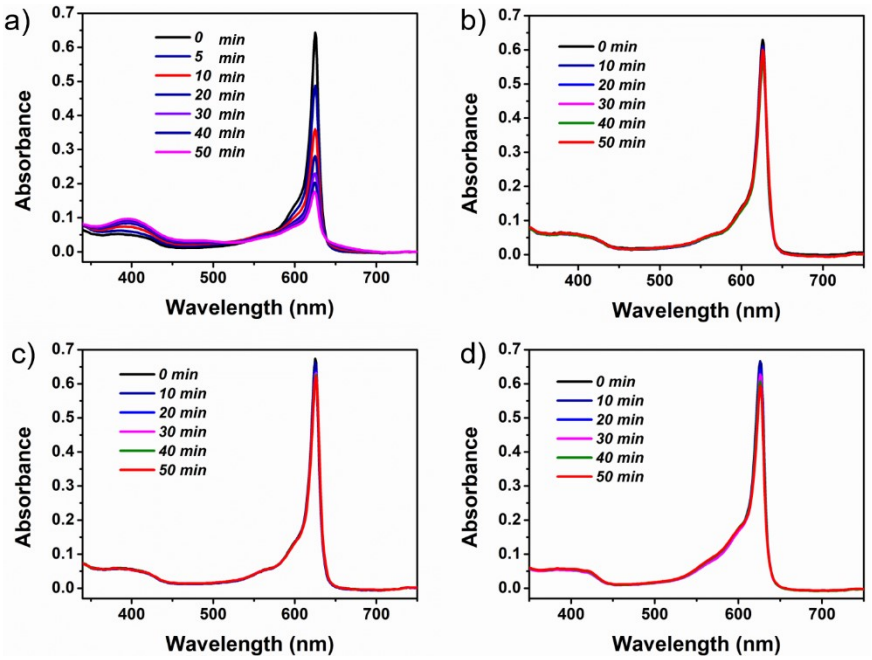

Figure S10. Time-dependent absorption responses of J-aggregated **BDP-Nit** (6 μM) to (a) NaHS (100 μM), (b) Cys (1mM), (c) Hcy (1mM), and (d) GSH (10 mM) in PBS.

(3) The impact of pH on the responsiveness:

The effect of pH on the H_2S-responsive ability was also evaluated. The absorption band of BDP-Nit nano assemblies at 623 nm was recorded in the presence of H_2S. As displayed Figure S11, the addition of H_2S induced the obvious decrease in the absorption in all groups. However, the responsive rate was increased with the decreasing of pH. The decreased pH would cause a positive increase of the zeta potential due to the protonation of pyridine functional group. We thus speculate the enhanced responsiveness effect was attribute to the highly positive charge surface of BDP-Nit nano assemblies which may enriches the local concentrations of HS^- (main forms of H_2S in physiological pH) to BDP-Nit to accelerate responsiveness (nucleophilic aromatic substitution). Meanwhile, the H_2S-activatable photosensitization was also examined by using non-emissive 2`,7`-dichlorodihydrofluorescein (DCFH), which will respond to ROS by the increased emission intensity at 526 nm. As shown in Figure S12, with the decreasing of pH, the fluorescence intensity changes of the probe at 526 nm in the presence of activated BDP-Nit assemblies was increased upon exposure to irradiation at same concentration. These should be favorable characteristics of BDP-Nit assemblies as the environment in tumor is markedly acidic.

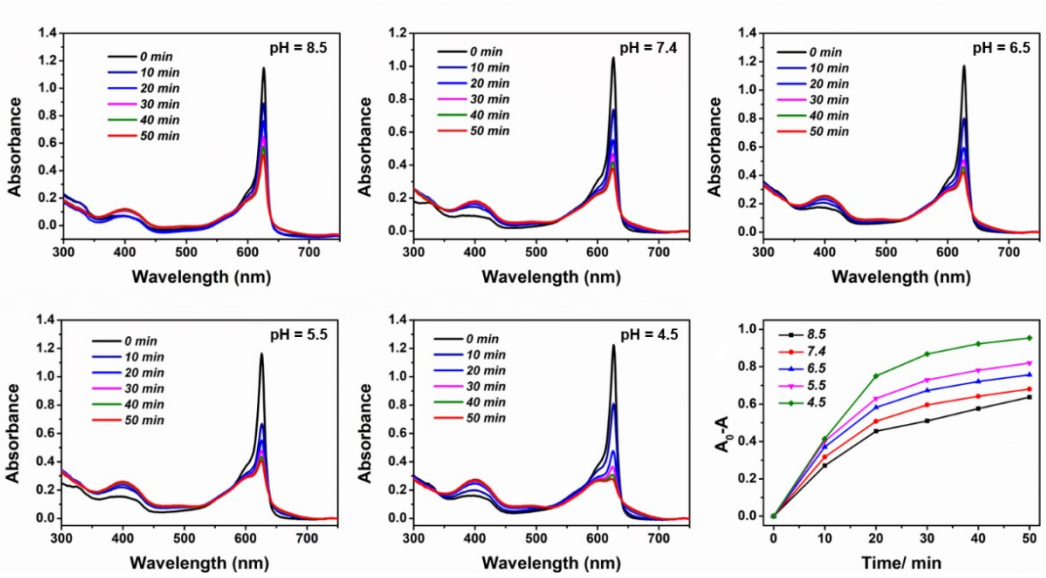

Figure S11. Time-dependent absorption changes of the J-aggregated BDP-Nit upon addition of NaSH (100 μM) for varying time intervals at different pH.

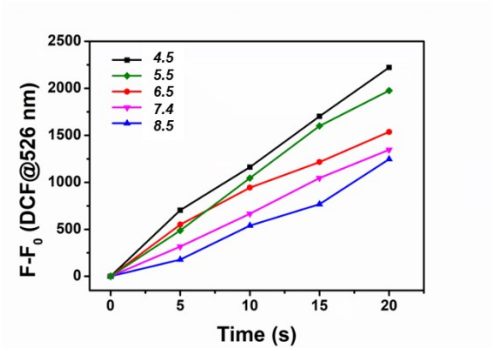

Figure S12. Fluorescence emission spectra of DCF upon light irradiation in the presence of NaSH-treated nano-assemblies for varying time intervals (0-20 s) at different pH. Light source: white light, 30 mW/cm^{-2}.

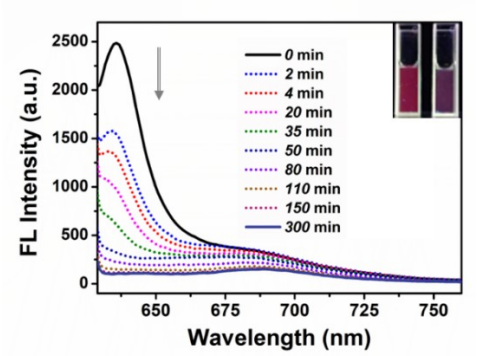

Figure S13. Time-dependent fluorescence changes of nano-assemblies in the aqueous solution in (a) present of NaSH (100 μM) for varying time intervals (0-5 h) at 37 °C.

5. HRMS spectra of the mixtures of BDP-Nit and Reactive sulfur species

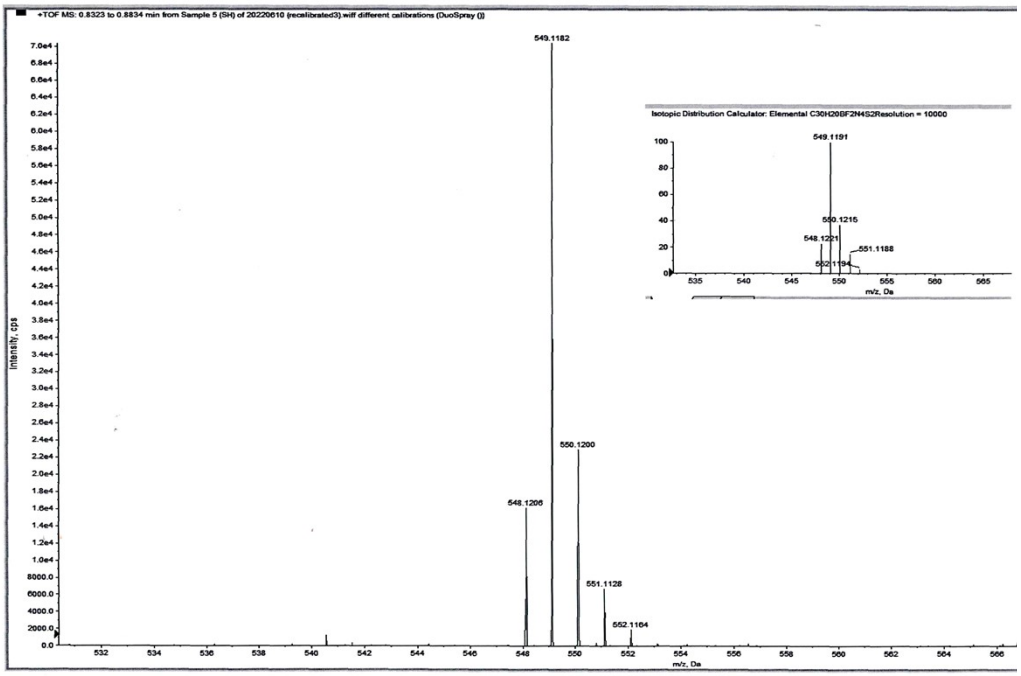

Figure S14. HRMS spectra of the mixtures of **BDP-Nit** and NaSH. The mixture of **BDP-Nit** and NaSH manifested a mass peak at 549.1182 identical to $[BODIPY\text{-}SH]^+$.

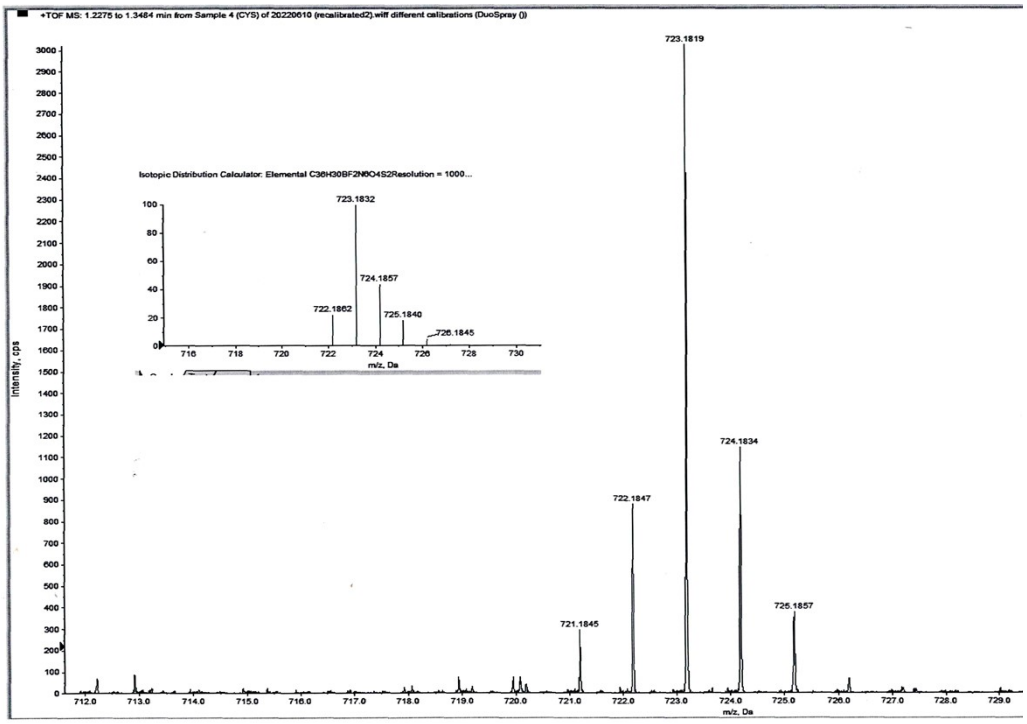

Figure S15. HRMS spectra of the mixtures of **BDP-Nit** and Cys. The mixture of **BDP-Nit** and Cys manifested a mass peak at 723.1819 identical to $[BODIPY\text{- }Cys]^{+}$.

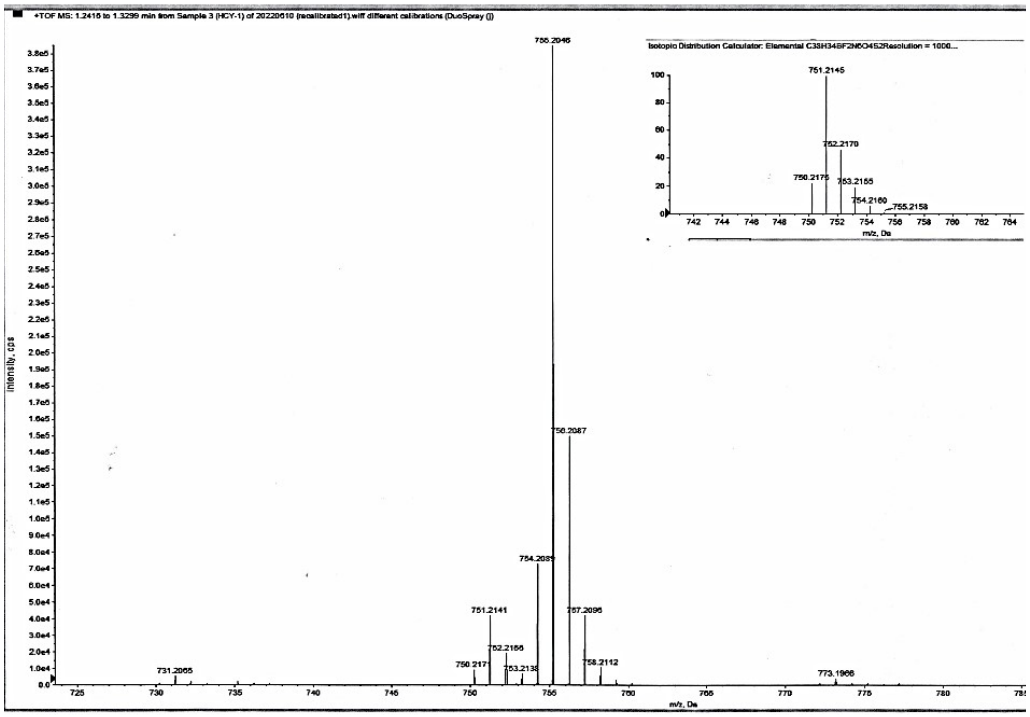

Figure S16. HRMS spectra of the mixtures of **BDP-Nit** and Hcy. The mixture of **BDP-Nit** and Hcy manifested a mass peak at 751.2141 identical to $[BODIPY\text{- }Hcy]^{+}$.

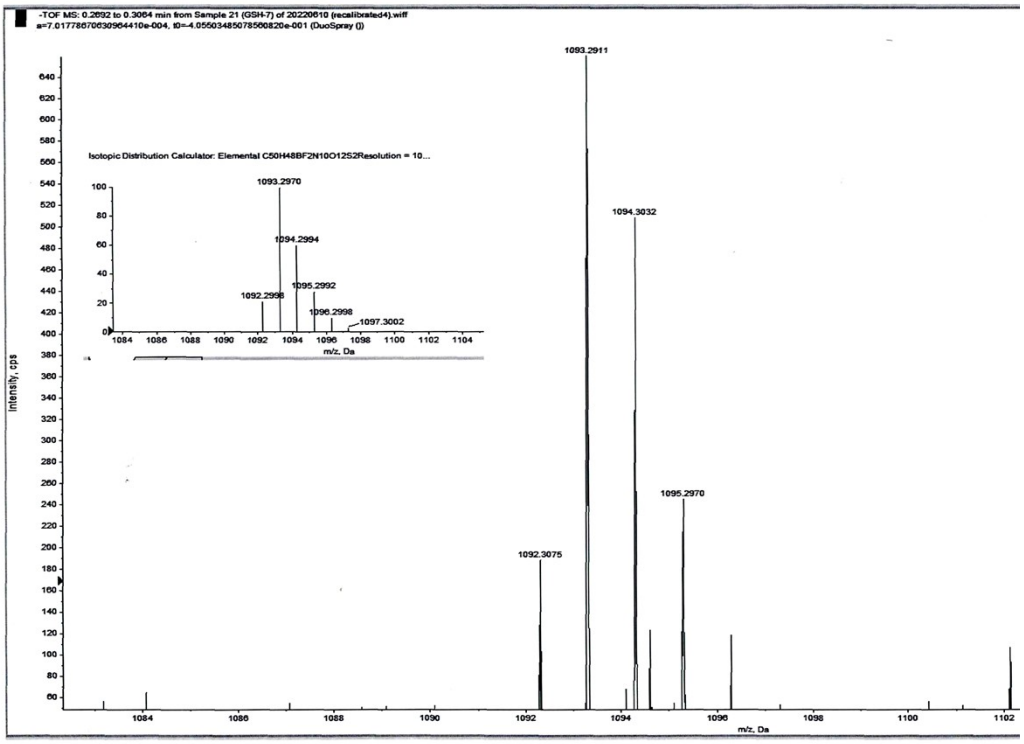

Figure S17. HRMS spectra of the mixtures of **BDP-Nit** and GSH. The mixture of **BDP-Nit** and GSH manifested a mass peak at 1093.2911 identical to $[BODIPY\text{- }GSH]^-$.

6. Photosensitivity assessment

The photosensitivity of the **BDP-SH**, **BDP-Nit** and the mixture of **BDP-Nit**/biothiols were explored using 2`,7`-dichlorodihydrofluorescein (DCFH) as a ROS indicator which will respond to ROS by the increased of emission intensity at 526 nm.

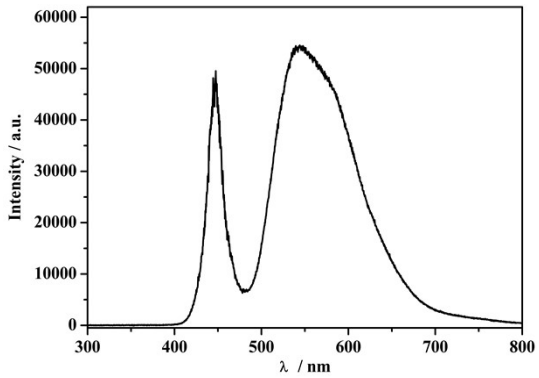

Figure S18. The UV-vis emission of the LED light.

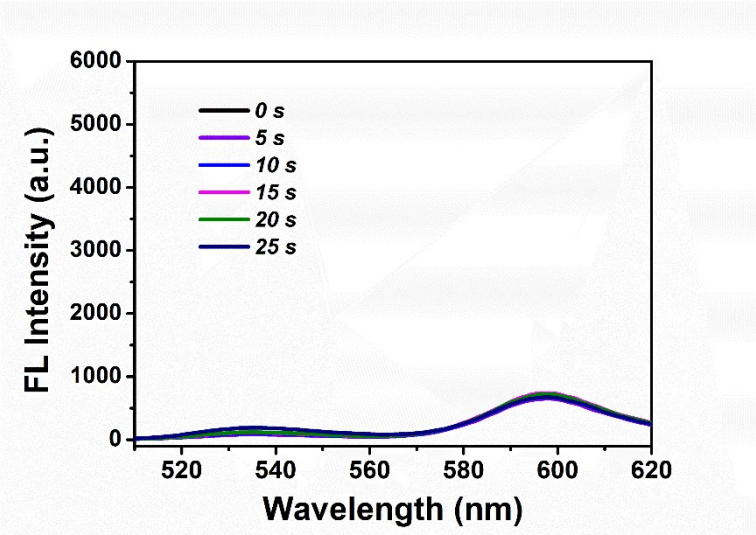

Figure S19. Fluorescence intensity of DCF after irradiation (white light, 30 mW/cm^2) for 25 s in the present of **BDP-Nit** in MeOH/H_2O (4:1, v/v).

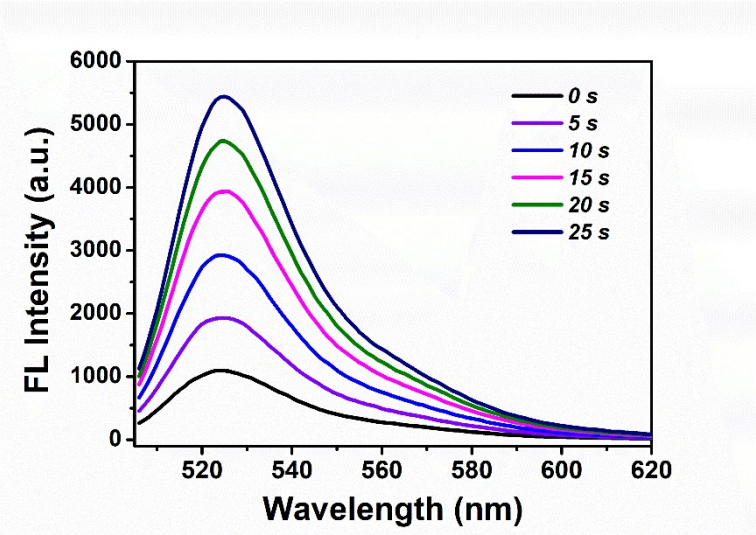

Figure S20. Fluorescence intensity of DCF after irradiation (white light, 30 mW/cm^2) for 25 s in the present of **BDP-SH** in MeOH/H_2O (4:1, v/v).

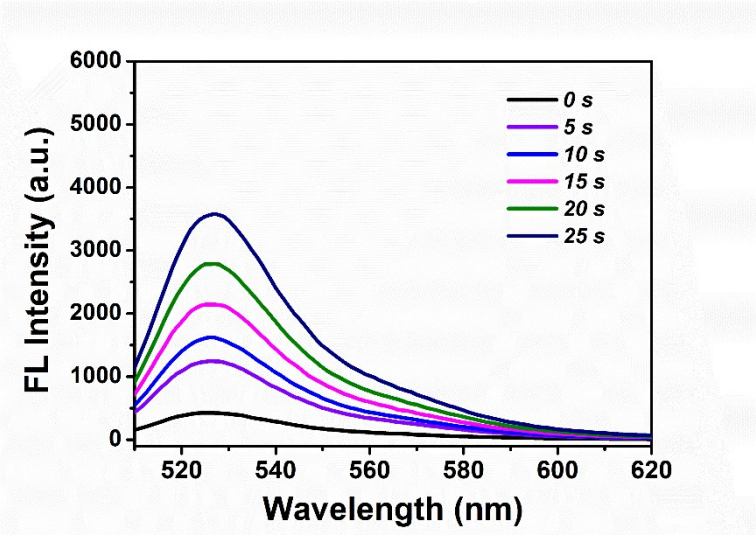

Figure S21. Fluorescence intensity of DCF after irradiation (white light, 30 mW/cm^2) for 25 s in the present of the mixture of **BDP-Nit** and GSH in MeOH/H_2O (4:1, v/v).

7. Experimental data in living cells

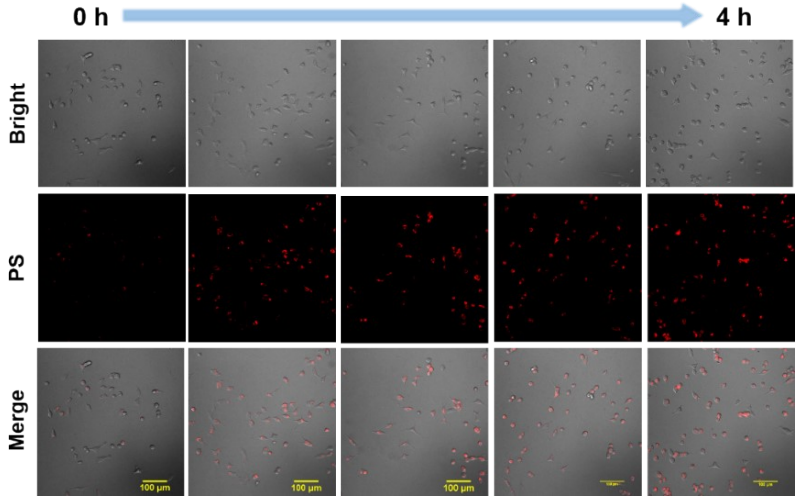

Figure S22. TP confocal fluorescence imaging for HeLa cells after treatment with nano-assemblies (10 mM) for different times (0, 1.0, 2.0, 3.0, 4.0, 5.0 and 6.0 h).

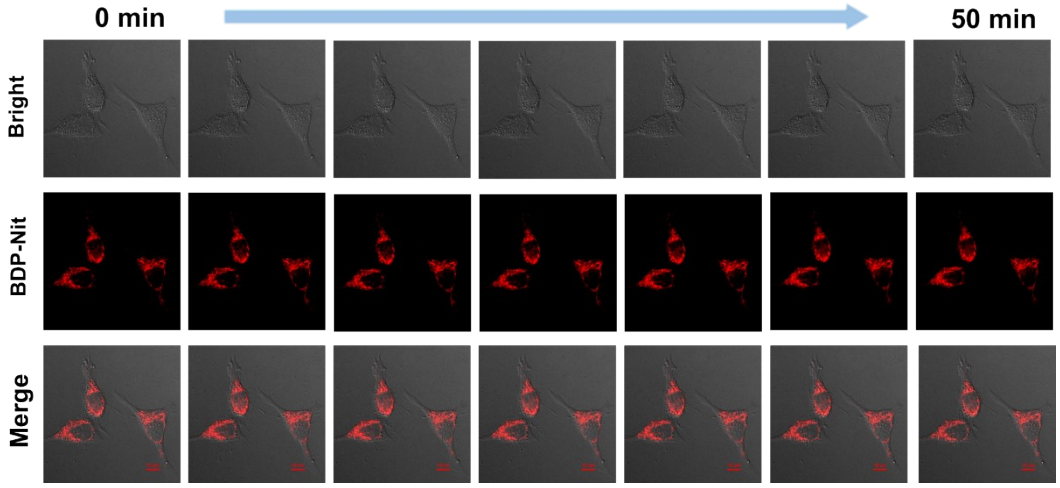

Figure S23. Fluorescence imaging of HeLa cell incubated nano-assemblies at varying time points in absence of NaSH over a period of 50 min.

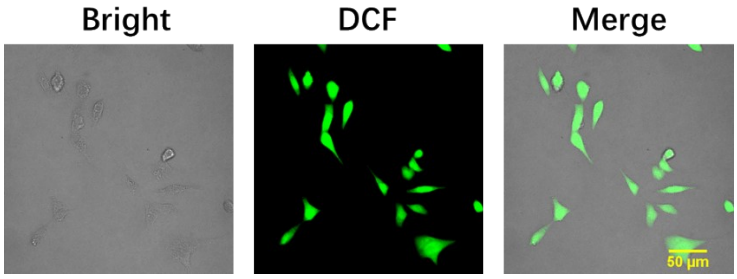

Figure S24. Fluorescence microscope images of HeLa cells after treatment with nano-assemblies (10 μM) loaded with DCFH-DA in present of NaSH (100 μM).

8. Crystal Growth and Characterization

Single crystal of BDP-Nit was obtained by slow solvent evaporation from the dye solution in CH_2Cl_2/n-heptane mixture. It's long-strip in shape with a length of 5~8 mm. We carefully cut it into small crystals, and picked out one of them with a suitable size (*ca.* 0.1 x 0.1 x 0.1 mm^3) for X-Ray analysis. Single crystal X-Ray diffraction data were collected at 100 K with a SuperNova Rigaku Oxford Diffraction diffractometers with Cu-Kα radiation. The crystallographic data are available at The Cambridge Crystallographic Data Center (CCDC 2178906).

Table S2. Crystal data and structure refinement.

CCDC number	2178906
Empirical formula	C43.5H28BCl3F2N6O6
Formula weight	885.88
Temperature/K	100.15
Crystal system	monoclinic
Space group	P21/n
a/Å	17.3763(3)
b/Å	9.1712(2)
c/Å	25.6188(5)
α/°	90

β/°	90.187(2)
γ/°	90
Volume/Å^3	4082.63(14)
Z	4
ρ_{calc} g/cm^3	1.441
μ/mm^{-1}	2.601
F (000)	1812.0
Radiation	CuKα (λ = 1.54184)
2Θ range for data collection/°	6.9 to 153.334
Reflections collected	8171
Independent reflections	8171
Data/restraints/parameters	8171/12/598
Goodness-of-fit on F^2	1.034
Final R indexes [I>=2σ (I)]	R1 = 0.0478, wR2 = 0.1121
Final R indexes [all data]	R1 = 0.0621, wR2 = 0.1197
Largest diff. peak/hole / e Å^{-3}	0.23/-0.25

Table S3. Anisotropic Displacement Parameters (Å^2×10^3). The Anisotropic displacement factor exponent takes the form: -2π^2[h^{2}a*^{2}U$_{11}$+2hka*b*U$_{12}$+…].

Atom	U_{11}	U_{22}	U_{33}	U_{23}	U_{13}	U_{12}
C017	24.1(9)	48.5(12)	28.4(10)	-8.3(9)	0.6(8)	0.0(9)
C018	40.7(11)	46.2(12)	24.1(9)	-4.8(9)	-2.4(8)	3.8(10)
C019	43.4(11)	34.0(11)	26.4(9)	2.8(8)	-2.7(8)	-2.1(9)
C21	33.1(10)	44.5(13)	35.2(11)	7.8(9)	9.3(9)	5.0(10)
C01B	37.4(11)	35.4(11)	38.6(11)	-7.3(9)	5.1(9)	0.4(9)
C01C	41.9(12)	30.0(11)	35.2(11)	4.2(9)	12.9(9)	9.1(9)
C01D	32.0(10)	41.4(12)	37.8(11)	-1.2(9)	6.3(9)	4.3(9)
C01E	37.6(11)	39.8(12)	32.9(11)	5.9(9)	9.4(9)	9.2(10)
C01F	37.7(11)	41.8(12)	39.6(12)	10.4(10)	9.0(9)	11.1(10)
C01G	36.8(11)	53.5(14)	23.6(9)	-3.5(9)	1.9(8)	3.3(10)
C01H	30.7(10)	66.5(16)	28.1(10)	2.3(10)	5.1(8)	0.4(11)
C01I	25.5(10)	73.4(16)	24.9(10)	1.5(10)	-0.8(8)	0.3(10)
C01J	55.9(14)	35.1(12)	36.1(11)	-11.0(10)	-12.8(10)	7.6(10)
C01K	50.8(13)	37.2(12)	44.0(13)	13.0(10)	14.0(11)	13.0(11)
C01L	71.1(17)	34.8(12)	33.2(11)	6.5(9)	1.9(11)	2.5(12)
C01M	47.6(13)	71.5(17)	24.2(10)	-4.7(11)	2.3(9)	-6.2(12)
C01N	64.1(16)	37.1(12)	40.7(12)	-7.9(10)	-1.7(11)	2.4(12)
C01O	80.4(19)	39.9(13)	34.8(12)	1.0(10)	-1.1(12)	-4.6(13)
B01P	26.5(10)	41.5(13)	22.5(10)	0.5(9)	0.1(8)	-6.6(9)
C22	62(4)	87(7)	38(4)	1(4)	-7(3)	-4(4)
Cl1	48.5(10)	61.7(14)	43.7(8)	3.6(9)	11.6(8)	-5.0(8)
Cl	137(6)	80(4)	67(3)	-8(3)	41(3)	-7(3)
Cl2	84(4)	82(4)	157(8)	-43(4)	-25(3)	16(2)
C22A	41(5)	74(8)	36(6)	7(5)	-3(4)	18(4)
C3	48(5)	34(4)	53(4)	5(3)	9(3)	-1(3)
Cl01	63.5(15)	75.4(17)	47.9(10)	9.4(10)	7.4(9)	6.1(10)

Cl02	39.5(12)	135(3)	71.9(18)	-43.2(14)	-9.7(7)	9.3(12)
F004	37.4(6)	44.1(7)	25.8(5)	-0.4(5)	9.7(5)	-9.0(5)
F005	33.6(6)	46.7(7)	33.4(6)	1.3(5)	-9.9(5)	-7.6(5)
Cl00	47.2(6)	45.9(6)	52.5(7)	3.6(6)	9.5(5)	-13.6(5)
O007	30.2(7)	46.6(9)	26.7(7)	-2.2(6)	4.6(6)	-10.8(6)
O008	32.4(7)	43.4(8)	28.4(7)	2.7(6)	-2.5(6)	-11.3(6)
O009	32.1(8)	70.3(11)	41.5(9)	16.1(8)	-0.6(7)	-3.7(8)
O00A	49.4(9)	62.0(11)	34.2(8)	4.2(8)	-12.8(7)	-6.4(8)
O10	75.0(12)	45.9(9)	34.2(8)	10.6(7)	-2.6(8)	-20.0(9)
N00C	23.9(7)	42.7(10)	23.5(8)	-0.3(7)	0.5(6)	-7.4(7)
N00D	24.9(8)	45.3(10)	21.4(7)	-0.3(7)	2.3(6)	-6.5(7)
N3	36.0(9)	48.7(11)	29.3(9)	13.1(8)	-5.5(7)	-1.8(8)
N2	51.1(12)	43.7(11)	31.1(9)	2.5(8)	2.1(8)	-15.1(9)
O00G	46.1(10)	81.4(14)	60.4(11)	19.2(10)	-3.3(9)	-23.8(10)
N00H	40.6(10)	38.7(10)	46.2(11)	-12.3(9)	-0.2(8)	1.8(8)
N1	73.3(15)	31.1(10)	39.8(11)	0.7(8)	13.1(10)	3.2(10)
C00J	24.6(9)	41.5(12)	25.6(9)	-0.4(8)	-0.3(7)	-3.1(8)
C00K	29.0(9)	30.3(10)	27.3(9)	3.7(8)	2.8(7)	-3.4(8)
C00L	40.4(11)	29.6(10)	27.2(9)	-2.6(8)	2.1(8)	-6.3(9)
C00M	22.0(9)	50.1(13)	23.6(9)	-2.0(9)	0.2(7)	-2.5(9)
C00N	25.2(9)	40.7(11)	26.9(9)	0.7(8)	4.2(7)	-5.0(8)
C00O	28.9(10)	32.4(11)	39.7(11)	-11.4(9)	-6.8(8)	6.9(8)
C00P	31.5(9)	30.5(10)	25.9(9)	-2.8(8)	-0.4(7)	-5.5(8)
C00Q	32.1(10)	26.7(10)	30.4(10)	2.6(8)	0.0(8)	0.6(8)
C00R	22.1(9)	52.9(13)	21.8(9)	2.8(9)	1.2(7)	-2.4(9)
C00S	24.4(9)	51.6(13)	27.4(10)	8.4(9)	3.2(8)	3.2(9)
C00T	30.3(10)	36.5(11)	27.3(9)	8.1(8)	-1.5(8)	-2.9(8)
C00U	24.3(9)	39.6(12)	34.5(10)	-7.0(9)	-0.5(8)	1.4(8)
C00V	31.2(10)	32.7(11)	32.0(10)	0.5(8)	-1.0(8)	-1.4(9)
C00W	26.5(9)	50.0(13)	27.0(10)	-1.9(9)	1.5(8)	1.5(9)
C00X	25.8(9)	56.6(14)	23.4(9)	0.9(9)	1.3(7)	-0.3(9)
C00Y	27.2(9)	41.5(12)	32.8(10)	5.4(9)	6.8(8)	1.6(9)
C00Z	30.8(10)	50.3(13)	26.5(10)	-4.4(9)	-2.4(8)	3.6(9)
C010	28.9(10)	44.2(12)	40.3(12)	-18.0(10)	-3.6(8)	1.5(9)
C011	34.8(10)	39.1(11)	29.4(10)	-1.0(9)	-5.9(8)	-2.4(9)
C012	18.6(8)	55.3(13)	25.3(9)	0.7(9)	0.5(7)	-0.7(9)
C013	31.3(10)	40.4(12)	35.2(11)	-10.2(9)	-3.3(8)	4.7(9)
C20	28.4(10)	43.1(13)	34.1(11)	-9.0(9)	-3.4(8)	3.7(9)
C015	33.1(10)	38.8(12)	36.6(11)	-9.9(9)	-5.1(9)	5.5(9)
C016	33.1(10)	47.1(12)	23.7(9)	-3.5(9)	3.9(8)	4.1(9)
C017	24.1(9)	48.5(12)	28.4(10)	-8.3(9)	0.6(8)	0.0(9)
C018	40.7(11)	46.2(12)	24.1(9)	-4.8(9)	-2.4(8)	3.8(10)
C019	43.4(11)	34.0(11)	26.4(9)	2.8(8)	-2.7(8)	-2.1(9)
C21	33.1(10)	44.5(13)	35.2(11)	7.8(9)	9.3(9)	5.0(10)
C01B	37.4(11)	35.4(11)	38.6(11)	-7.3(9)	5.1(9)	0.4(9)
C01C	41.9(12)	30.0(11)	35.2(11)	4.2(9)	12.9(9)	9.1(9)
C01D	32.0(10)	41.4(12)	37.8(11)	-1.2(9)	6.3(9)	4.3(9)
C01E	37.6(11)	39.8(12)	32.9(11)	5.9(9)	9.4(9)	9.2(10)

C01F	37.7(11)	41.8(12)	39.6(12)	10.4(10)	9.0(9)	11.1(10)
C01G	36.8(11)	53.5(14)	23.6(9)	-3.5(9)	1.9(8)	3.3(10)
C01H	30.7(10)	66.5(16)	28.1(10)	2.3(10)	5.1(8)	0.4(11)
C01I	25.5(10)	73.4(16)	24.9(10)	1.5(10)	-0.8(8)	0.3(10)
C01J	55.9(14)	35.1(12)	36.1(11)	-11.0(10)	-12.8(10)	7.6(10)
C01K	50.8(13)	37.2(12)	44.0(13)	13.0(10)	14.0(11)	13.0(11)
C01L	71.1(17)	34.8(12)	33.2(11)	6.5(9)	1.9(11)	2.5(12)
C01M	47.6(13)	71.5(17)	24.2(10)	-4.7(11)	2.3(9)	-6.2(12)
C01N	64.1(16)	37.1(12)	40.7(12)	-7.9(10)	-1.7(11)	2.4(12)
C01O	80.4(19)	39.9(13)	34.8(12)	1.0(10)	-1.1(12)	-4.6(13)
B01P	26.5(10)	41.5(13)	22.5(10)	0.5(9)	0.1(8)	-6.6(9)
C22	62(4)	87(7)	38(4)	1(4)	-7(3)	-4(4)
Cl1	48.5(10)	61.7(14)	43.7(8)	3.6(9)	11.6(8)	-5.0(8)
Cl	137(6)	80(4)	67(3)	-8(3)	41(3)	-7(3)
Cl2	84(4)	82(4)	157(8)	-43(4)	-25(3)	16(2)
C22A	41(5)	74(8)	36(6)	7(5)	-3(4)	18(4)
C3	48(5)	34(4)	53(4)	5(3)	9(3)	-1(3)

9. Reference

1. B. Ventura, G. Marconi, M. Bröring, R. Krüger and L. Flamigni, *New J. Chem.*, 2009, **33**, 428-438.